Correspondence to:

Professor M.G. Humphrey

Research School of Chemistry

Australian National University

Canberra, ACT 2601

Australia

T: +61 2 6125 2927

F: +61 2 6125 0750

E: Mark.Humphrey@anu.edu.au

Contribution to the Special Issue of the Journal of Organometallic Chemistry on Advances in Di- and Polynuclear Organometallic Complexes, dedicated in Memoriam to Professor Jack Lewis

Mixed-Metal Cluster Chemistry. 37. Syntheses, Structural, Spectroscopic, Electrochemical, and Optical Power Limiting Studies of Tetranuclear Molybdenum-Iridium Clusters

Junhong Fu, Graeme J. Moxey, Mahbod Morshedi, Adam Barlow, Michael D. Randles, Peter V. Simpson, Torsten Schwich, Marie P. Cifuentes, and Mark G. Humphrey*

Research School of Chemistry, Australian National University, Canberra, ACT 2601, Australia.

* Correspondence author. Ph: +61 2 6125 2927; Fax: +61 2 6125 0750; email: Mark.Humphrey@anu.edu.au

Dedicated to Professor Jack Lewis, a cluster chemist par excellence.

Abstract

Tetrahedral $Mo_2Ir_2(\mu_3\text{-}CO)(\mu\text{-}CO)_5(CO)_4(\eta^5\text{-}C_5H_5)_2$ (**1**) reacted with $P(C_6H_4Me\text{-}4)_3$, $P(C_6H_2Me_2\text{-}3,5\text{-}OMe\text{-}4)_3$, and $AsPh_3$ to afford the substitution products $Mo_2Ir_2(\mu\text{-}CO)_3(CO)_6(L)(\eta^5\text{-}C_5H_5)_2$ [L = $P(C_6H_4Me\text{-}4)_3$ (**3**), $P(C_6H_2Me_2\text{-}3,5\text{-}OMe\text{-}4)_3$ (**4**), $AsPh_3$ (**5**)] in fair to good yields, while reaction of **1** with $HC\alpha CSiPr^i_3$ proceeded by insertion into the Mo-Mo bond to give the pseudo-octahedral $Mo_2Ir_2(\mu_4\text{-}\eta^2\text{-}HC_2SiPr^i_3)(\mu\text{-}CO)_4(CO)_4(\eta^5\text{-}C_5H_5)_2$ (**6**) in fair yield. While $MoIr_3(\mu\text{-}CO)_3(CO)_7(\eta^5\text{-}C_5H_5)$ reacted with $HC\alpha CSiMe_3$ to give a complex mixture of thus-far-uncharacterized products, its phosphine substitution product $MoIr_3(\mu\text{-}CO)_3(CO)_5(PPh_3)_2(\eta^5\text{-}C_5H_5)$ reacted with the same alkyne via insertion into a Mo-Ir bond to afford the pseudo-octahedral $MoIr_3(\mu_4\text{-}\eta^2\text{-}HC_2SiMe_3)(\mu\text{-}CO)_3(CO)_4(PPh_3)_2(\eta^5\text{-}C_5H_5)$ (**8**) in good yield. Clusters **4**, **5** (two isomers), **6** and **8** have been characterized by single-crystal X-ray diffraction studies. Cyclic voltammetric studies of $Mo_2Ir_2(\mu\text{-}CO)_3(CO)_6(PPh_3)(\eta^5\text{-}C_5H_5)_2$ (**2**), **3**-**6** and **8** confirmed the tuning of redox potentials upon phosphines/arsine introduction and alkyne modification. IR spectroelectrochemical studies of **2**, **6**, and **8** suggest decreasing proclivity for bridging carbonyl ligands following oxidation. Variable temperature ^{31}P NMR studies of **3** and **4** revealed interconverting isomers in solution, the structures of which are assigned as analogues of the X-ray diffraction-confirmed isomers of **5**. Studies of **2**-**5** using ns pulses and the open-aperture Z-scan technique revealed that all are optical limiters at wavelengths in the visible region.

Keywords: Crystal structures; Molybdenum; Iridium; Cluster; Cyclopentadienyl

1. Introduction

Pioneering studies carried out by the Lewis group and others in the 1960s and 1970s established metal carbonyl cluster chemistry as a vibrant research field, unveiling a diverse array of structures, bonding modes, and reactivity patterns with these aesthetically appealing species [1,2]. The majority of the early reports focused on homonuclear clusters, because these are frequently accessible by simple thermolyses of low-nuclearity or mononuclear precursors. The somewhat later growth of mixed-metal cluster chemistry followed the development of rational routes to heteronuclear clusters [3-5], the resultant complexes possessing several interesting features (e.g. polar M-M' linkages that potentially facilitate organic substrate activation, differing metal centres that can "select" for specific reagents, and the possibility of such species either functioning as homogeneous heterobimetallic catalysts or precursors to heterogeneous heterobimetallic catalysts with precise control of the metal disposition) [6].

We have previously reported studies of the phosphine and alkyne chemistry of the tetrahedral molybdenum-iridium carbonyl clusters $MoIr_3(\mu\text{-}CO)_3(CO)_7(\eta^5\text{-}C_5H_5)$ and $Mo_2Ir_2(\mu_3\text{-}CO)(\mu\text{-}CO)_5(CO)_4(\eta^5\text{-}C_5H_5)_2$ and related clusters possessing varying degrees of cyclopentadienyl alkylation [7-16]. In continuing studies of this system, we report, inter alia, alkyne chemistry at a phosphine-substituted cluster that proceeds via a differing pathway to its non-phosphine-substituted analogue, electrochemical studies of phosphine- and alkyne-functionalized derivatives confirming that cluster electron richness can be tuned systematically, spectroelectrochemical studies revealing that oxidation disfavours bridging carbonyls in this system, and Z-scan

studies of systematically-substituted examples that explore the impact of phosphine ligation on optical limiting merit.

2. Experimental

2.1. General experimental conditions and starting materials

Reactions were performed under an atmosphere of nitrogen using standard Schlenk techniques, although no special precautions were taken to exclude air in the work-ups. Reactions were monitored regularly by IR spectroscopy to ensure consumption of the starting cluster. Dichloromethane used in reactions was AR grade and distilled over CaH_2 under nitrogen. All other solvents and other reagents were obtained commercially and were used as received. Petrol refers to a fraction of boiling range 60 – 80 °C. Cluster products were purified by preparative thin-layer chromatography (TLC) on 20 × 20 cm glass plates coated with Merck GF_{254} silica gel (0.5 mm). Analytical TLC was conducted on aluminum sheets coated with 0.25 mm Merck GF_{254} silica gel. Literature procedures were used to synthesize $Mo_2Ir_2(\mu_3\text{-}CO)(\mu\text{-}CO)_5(CO)_4(\eta^5\text{-}C_5H_5)_2$ (**1**) [7], $MoIr_3(\mu\text{-}CO)_3(CO)_8(\eta^5\text{-}C_5H_5)$ [17], $Mo_2Ir_2(\mu\text{-}CO)_3(CO)_6(PPh_3)(\eta^5\text{-}C_5H_5)_2$ (**2**), and $MoIr_3(\mu\text{-}CO)_3(CO)_6(PPh_3)_2(\eta^5\text{-}C_5H_5)$ (**7**) [8]. $P(C_6H_4Me\text{-}4)_3$, $P(C_6H_2Me_2\text{-}3,5\text{-}OMe\text{-}4)_3$, $AsPh_3$, $HC{\equiv}CSiMe_3$, and $HC{\equiv}CSiPr^i_3$ were obtained commercially and were used as received.

2.2. Instrumentation

Infrared spectra were recorded on PerkinElmer System 2000 and PerkinElmer Spectrum One FT-IR spectrometers using a CaF_2 solution cell and AR grade CH_2Cl_2 solvent; spectral features are reported in cm^{-1}. ^1H NMR spectra were recorded on a Bruker Ascend-400 spectrometer at 400 MHz in $CDCl_3$ (Cambridge Isotope Laboratories) and referenced to non-deuterated solvent (δ 7.26). Variable-temperature ^{31}P NMR spectra were recorded on a Bruker Ascend-400 spectrometer at 162 MHz, Varian Inova-500 spectrometer at 202 MHz, or a Bruker Avance spectrometer at 324 MHz in $CDCl_3$, CD_2Cl_2 or toluene-d_8. Unit resolution and high-resolution ESI mass spectra were recorded on a Micromass-Waters LC-ZMD single quadrupole liquid chromatograph-MS instrument, and are reported in the form: *m*/*z* (assignment, relative intensity). Microanalyses were carried out at the School of Human Sciences, Science Centre, London Metropolitan University, UK. Cyclic voltammograms were recorded at room temperature using an EA161 potentiostat and e-corder from eDaq Pty Ltd, with 1 mm diameter platinum disk working, platinum wire auxiliary, and Ag/AgCl reference electrodes, such that the ferrocene/ferrocenium redox couple was located at 0.56 V (i_{pc}/i_{pa} = 1; ΔE_p = 0.09 V). Scan rates were typically 100 mV s^{-1}. Solutions contained 0.1 M $(NBu^n_4)PF_6$ and ca. 10^{-3} M complex in dried, distilled dichloromethane, and were deoxygenated and maintained under a nitrogen atmosphere. IR spectroelectrochemical data were recorded on a PerkinElmer Frontier FT-IR spectrometer. Solutions were made up using 0.3 M $(NBu^n_4)PF_6$ in dried and distilled dichloromethane. Solution spectra of the oxidized species were obtained at 298 K by electrogeneration with an applied potential of 700 mV in an optically transparent thin-layer electrochemical (OTTLE) cell.

*2.3. Synthesis of $Mo_2Ir_2(\mu\text{-}CO)_3(CO)_6\{P(C_6H_4Me\text{-}4)_3\}(\eta^5\text{-}C_5H_5)_2$ (**3**)*

$P(C_6H_4Me\text{-}4)_3$ (2.9 mg, 9.5 μmol) was added to an orange solution of $Mo_2Ir_2(\mu_3\text{-}CO)(\mu\text{-}CO)_5(CO)_4(\eta^5\text{-}C_5H_5)_2$ (**1**, 9.2 mg, 9.3 μmol) in CH_2Cl_2 (10 mL) and the resultant mixture was stirred for 23 h. The solution was taken to dryness in vacuo, and the crude residue dissolved in the minimum amount of CH_2Cl_2 and applied to a preparative silica TLC plate. Elution with CH_2Cl_2/petrol (9:1) afforded 1 band (R_f = 0.8, dark orange). Extraction with CH_2Cl_2 and reduction of the solvent volume afforded a brown solid identified as $Mo_2Ir_2(\mu\text{-}CO)_3(CO)_6\{P(C_6H_4Me\text{-}4)_3\}(\eta^5\text{-}C_5H_5)_2$ (**3**) (6.5 mg, 5.1 μmol, 56%). IR (CH_2Cl_2): ν(CO) 2037 s, 1991 vs, 1953 vw, 1915 s, 1857 m, 1823 m, 1746 m cm^{-1}. ^1H NMR ($CDCl_3$): δ 7.15-7.22 (m, 12H, C_6H_4), 4.67 (s, 10H, C_5H_5), 2.39 (s, 9H, Me). ^{31}P NMR ($CDCl_3$, 273 K): δ 14.5, 2.9. MS (ESI): calculated, $C_{40}H_{32}Ir_2Mo_2O_9P$, 1268.9151 ($[M + H]^+$); found, 1268.9164 ($[M + H]^+$, 5). Analysis calculated for $C_{40}H_{31}Ir_2Mo_2O_9P$: C 38.04, H 2.57 %: found, C 38.14, H 2.51%.

*2.4. Synthesis of $Mo_2Ir_2(\mu\text{-}CO)_3(CO)_6\{P(C_6H_2Me_2\text{-}3,5\text{-}OMe\text{-}4)_3\}(\eta^5\text{-}C_5H_5)_2$ (**4**)*

$P(C_6H_2Me_2\text{-}3,5\text{-}OMe\text{-}4)_3$ (4.2 mg, 9.6 μmol) was added to an orange solution of $Mo_2Ir_2(\mu_3\text{-}CO)(\mu\text{-}CO)_5(CO)_4(\eta^5\text{-}C_5H_5)_2$ (**1**, 9.3 mg, 9.4 μmol) in CH_2Cl_2 (10 mL) and the resultant mixture was stirred for 24 h. The solution was taken to dryness in vacuo, and the crude residue dissolved in the minimum amount of CH_2Cl_2 and applied to a preparative silica TLC plate. Elution with CH_2Cl_2/petrol (9:1) afforded 2 bands. The contents of the first band (R_f = 0.8, orange) were identified as unreacted **1** (1.3 mg, 1.3 μmol, 14%). The contents of the second band (R_f = 0.6, dark orange) were identified as $Mo_2Ir_2(\mu\text{-}CO)_3(CO)_6\{P(C_6H_2Me_2\text{-}3,5\text{-}OMe\text{-}4)_3\}(\eta^5\text{-}C_5H_5)_2$ (**4**) (6.8 mg, 4.9 μmol,

52%). IR (CH_2Cl_2): ν(CO) 2038 s, 1992 vs, 1954 vw, 1915 s, 1854 m, 1820 m, 1745 m cm^{-1}. ^1H NMR ($CDCl_3$): δ 6.98-7.08 (m, 6H, C_6H_2), 4.74 (s, 10H, C_5H_5), 3.73 (s, 9H, OMe), 2.23 (s, 18H, Me). ^{31}P NMR (toluene-d_8, 273 K): δ 13.5, -0.7. MS (ESI): calculated, $C_{46}H_{44}Ir_2Mo_2O_{12}P$, 1400.9937 ($[M + H]^+$); found, 1400.9908 ($[M + H]^+$, 5). Analysis calculated for $C_{46}H_{43}Ir_2Mo_2O_{12}P$: C 39.60, H 3.10 %: found, C 39.48, H 2.99%.

*2.5. Synthesis of $Mo_2Ir_2(\mu\text{-}CO)_3(AsPh_3)(CO)_6(\eta^5\text{-}C_5H_5)_2$ (**5**)*

$AsPh_3$ (2.6 mg, 8.5 μmol) was added to an orange solution of $Mo_2Ir_2(\mu_3\text{-}CO)(\mu\text{-}CO)_5(CO)_4(\eta^5\text{-}C_5H_5)_2$ (**1**, 7.9 mg, 8.0 μmol) in CH_2Cl_2 (15 mL) and the resultant mixture was stirred for 16 h. The solution was taken to dryness in vacuo, and the crude residue dissolved in the minimum amount of CH_2Cl_2 and applied to a preparative silica TLC plate. Elution with CH_2Cl_2 afforded 1 band (R_f = 0.9, dark orange). Extraction with CH_2Cl_2 and reduction of the solvent volume afforded a brown solid identified as $Mo_2Ir_2(\mu\text{-}CO)_3(AsPh_3)(CO)_6(\eta^5\text{-}C_5H_5)_2$ (**5**) (3.8 mg, 3.0 μmol, 38%). Two isomers, **5a** and **5b**, crystallized simultaneously and could not be separated. IR (CH_2Cl_2): ν(CO) 2037 s, 1990 vs, 1951 vw, 1918 m, 1861 m, 1826 m, 1747 m cm^{-1}. ^1H NMR: δ 7.38-7.45 (m, 15H, Ph), 4.81 (s, 10H, C_5H_5). MS (ESI): calculated, $C_{37}H_{25}Ir_2Mo_2NaO_9$, 1288.7932 ($[M + Na]^+$); found, 1288.7936 ($[M + Na]^+$, 6). Insufficient material precluded microanalysis.

*2.6. Synthesis of $Mo_2Ir_2(\mu_4\text{-}\eta^2\text{-}HC_2SiPr^i_3)(\mu\text{-}CO)_4(CO)_4(\eta^5\text{-}C_5H_5)_2$ (**6**)*

$HC{\equiv}CSiPr^i_3$ (0.01 mL, 89 μmol) was added to an orange solution of $Mo_2Ir_2(\mu_3\text{-}CO)(\mu\text{-}CO)_5(CO)_4(\eta^5\text{-}C_5H_5)_2$ (**1**, 16.0 mg, 16.1 μmol) in CH_2Cl_2 (5 mL) and the resultant

mixture was refluxed for 23 h. The solution was taken to dryness in vacuo, and the crude residue dissolved in the minimum amount of CH_2Cl_2 and applied to a preparative silica TLC plate. Elution with CH_2Cl_2/petrol (1:1) afforded 7 bands. The contents of the sixth band (R_f = 0.2, blue green) were identified as $Mo_2Ir_2(\mu_4\text{-}\eta^2\text{-}HC_2SiPr^i_3)(\mu\text{-}CO)_4(CO)_4(\eta^5\text{-}C_5H_5)_2$ (**6**) (4.5 mg, 4.0 μmol, 25%). IR (CH_2Cl_2): ν(CO) 2072 s, 2036 vs, 2013 w, 1991 sh, 1812 br, 1765 br cm^{-1}. ^1H NMR: δ 9.78 (s, 1H, HC_2), 5.36 (s, 10H, C_5H_5), 1.25 (m, 21H, $SiPr^i_3$). MS (ESI): calculated, $C_{29}H_{33}Ir_2Mo_2O_8Si$, 1118.9312 ($[M + H]^+$); found, 1118.9330 ($[M + H]^+$, 1). Insufficient material precluded microanalysis.

2.8. Reaction of $MoIr_3(\mu\text{-}CO)_3(CO)_8(\eta^5\text{-}C_5H_5)$ with $HC{\equiv}CSiMe_3$

$HC{\equiv}CSiMe_3$ (0.01 mL, 71 μmol) was added to an orange solution of $MoIr_3(\mu\text{-}CO)_3(CO)_8(\eta^5\text{-}C_5H_5)$ (15.5 mg, 14.7 μmol) in CH_2Cl_2 (5 mL) and the resultant mixture was stirred at room temperature for 18 h. The solution was taken to dryness in vacuo, and the crude residue dissolved in the minimum amount of CH_2Cl_2 and applied to a preparative silica TLC plate. Elution with 4:1 CH_2Cl_2:petrol afforded more than ten bands, the contents of which were all in trace amounts.

*2.9. Synthesis of $MoIr_3(\mu_4\text{-}\eta^2\text{-}HC_2SiMe_3)(\mu\text{-}CO)_3(CO)_4(PPh_3)_2(\eta^5\text{-}C_5H_5)$ (**8**)*

$HC{\equiv}CSiMe_3$ (0.01 mL, 71 μmol) was added to an orange solution of $MoIr_3(\mu\text{-}CO)_3(CO)_6(PPh_3)_2(\eta^5\text{-}C_5H_5)$ (**7**, 10.0 mg, 6.6 μmol) in CH_2Cl_2 (8 mL) and the resultant mixture was refluxed for 3 h. The solution was taken to dryness in vacuo, and the crude residue dissolved in the minimum amount of CH_2Cl_2 and applied to a

preparative silica TLC plate. Elution with CH_2Cl_2 afforded two bands. The contents of the first band (R_f = 0.7, orange) were identified as unreacted **7 (**1.2 mg, 0.8 μmol, 12%**)**. The contents of the second band (R_f = 0.3, green) were identified as $MoIr_3(\mu_4\text{-}\eta^2\text{-}HC_2SiMe_3)(\mu\text{-}CO)_3(CO)_4(PPh_3)_2(\eta^5\text{-}C_5H_5)$ (**8**) (4.4 mg, 2.8 μmol, 43%). IR (CH_2Cl_2): ν(CO) 2032 s, 2003 s, 1972 sh, 1786 m, 1733 s cm^{-1}. ^1H NMR: δ 7.65 (dd, 1H, J_{PH} = 14, 3 Hz, HC_2), 7.20-7.39 (m, 30H, Ph), 4.69 (s, 5H, C_5H_5), -0.22 (s, 9H, $SiMe_3$). ^{31}P NMR: δ 5.1, -4.9. MS (ESI): calculated, $C_{45}H_{46}Ir_3MoO_7P_2Si$, 1561.0430 ($[M + H]^+$); found, 1561.0464 ($[M + H]^+$, 20). Insufficient material precluded microanalysis.

2.10. X-ray structural studies

The crystal and refinement data for compounds **4**, **5a**, **5b**, **6** and **8** are summarized in Table 1. Selected bond distances for **4**, **5a** and **5b** are listed in Table 2, and selected bond distances for **6** and **8** are listed in Table 3. Crystals suitable for the X-ray structural analyses were grown by carefully layering a hexane solution onto methanol (**4**, **5a**, **5b**) or by liquid diffusion of methanol into a dichloromethane solution (**6**, **8**) at 277 K. Suitable crystals were mounted on fine glass capillaries, and intensity data were collected on a Nonius KAPPA CCD diffractometer at 200 K using graphite-monochromated Mo-Kα radiation (λ = 0.71073 Å). N_t (total) reflections were measured by using psi and omega scans and were reduced to N_o unique reflections, with $F_o > 2\sigma(F_o)$ being considered to be observed. Semi-empirical absorption corrections based on symmetry-equivalent and repeat reflections (**4**, **5a**, **5b**, **8**) or Gaussian grid face-indexed absorption corrections (**6**) were applied [18,19]. The structures were solved using direct methods and observed reflections were used in

least-squares refinement on F^2, with anisotropic thermal parameters refined for non-hydrogen atoms. Hydrogen atoms were constrained in calculated positions and refined with a riding model. Structure solutions and refinements were performed by using the programs SHELXS-97 [20] and SHELXL-2013 [21] through the graphical interface Olex2 [22], which was also used to generate the figures. In all structures, the largest peaks in the final difference electron map are located near the metal atoms. Crystallographic data for the structural analyses have been deposited with the Cambridge Crystallographic Data Centre, CCDC numbers 1402682-1402686. Copies of this information may be obtained, free of charge, from the Director, CCDC, 12 Union Road, Cambridge CB2 1E2, UK (fax: +44-1223-336033; e-mail: deposit@ccdc.cam.ac.uk or www: *http://www.ccdc.cam.ac.uk*). Variata. In **4**, rigid-bond restraints were applied to atoms C101-C106, C110-C115 and C119-C124 of the phosphine ligand, and atoms C301-C305 and C401-C405 of the cyclopentadienyl ligands. Anisotropic displacement parameter restraints were applied to atoms C21, O21, C42 and O42 (carbonyl ligands) and C101-C106 (phosphine ligand). In **5a**, rigid-bond restraints and bond distance restraints were applied to atoms C301-C305 of the cyclopentadienyl ligand. Disordered lattice solvent (methanol) was removed from the refinement using PLATON SQUEEZE [23]. In **5b**, rigid-bond restraints were applied to atoms C301-C305 of the cyclopentadienyl ligand. In **6**, the alkynyl hydrogen atom (H134) was located from the Fourier difference map and was refined isotropically. Disordered lattice solvent (dichloromethane) was removed from the refinement using PLATON SQUEEZE [23]. In **8**, the alkynyl hydrogen atom (H134) was located from the Fourier difference map and was refined isotropically.

2.11. Optical limiting studies

The light source used for the determination of power limiting properties was an Opolette (HE) 355 II (Opotek) single-housing tuneable ns laser system, with a flashlamp-pumped Nd:YAG laser (355 nm pump wavelength, 20 Hz repetition rate, 5 ns pulse length) pumping an OPO (tuning range 410-2200 nm, peak OPO energy 10 mJ, spectral linewidth 4-7 cm^{-1}). The optical power limiting experiments were performed on solutions of concentrations sufficient to permit ~ 70 % light transmission through the sample (actual concentrations employed are listed in Table 4). The laser power was moderated using neutral density filters to prevent sample decomposition during the scan.

The Z-scan method was used to obtain the nonlinear transmission plots of the samples, which were then transformed to fluence plots by measuring the power level (using a power meter) and the beam radius calculated using:

$$w_z = w_0(1 + \frac{z^2}{z_r^2})$$

the beam waist and Rayleigh length being obtained from fitting the closed-aperture trace obtained for a fused silica plate (found to be between 47 and 49 μm). From these plots, ground-state and "effective" excited-state cross-sections (σ_0 and σ_{eff}, respectively) were obtained, assuming three-state reverse saturable absorption and using the following literature expressions:

$$T = \frac{(1-R)^2 \exp(-\alpha_0 L)}{q} Ln(1+q)$$

where:

$$q = \frac{(1-R)[1-\exp(-\alpha_0 L)]\delta_{eff} F_0}{2F_s}$$

and:

$$\delta_{eff} = \frac{\sigma_{eff}-\sigma_0}{\sigma_0} \qquad F_s = \frac{\hbar\omega}{\sigma_0}$$

The magnitude of the total nonlinear absorption (β_{eff}) was calculated by the fitting of an ideal curve to the normalized open-aperture Z-scan data using the following expressions:

$$T(z) = 1 - \frac{q_0}{2\sqrt{2}} \quad \text{for} \quad q_0 < 1$$

where:

$$q_0 = \frac{\beta_{eff} I_0 (1 - e^{-\alpha L})}{(1 + \left(\frac{z}{z_r}\right)^2)\alpha}$$

3. Results and discussion

*3.1. Syntheses of **3**-**5** and structural studies of **4** and **5***

We have previously reported the synthesis of $Mo_2Ir_2(\mu\text{-}CO)_3(CO)_6(PPh_3)(\eta^5\text{-}C_5H_5)_2$ (**2**) from reaction of $Mo_2Ir_2(\mu_3\text{-}CO)(\mu\text{-}CO)_5(CO)_4(\eta^5\text{-}C_5H_5)_2$ (**1**) and PPh_3 in dichloromethane at room temperature [8]. In the present studies, the analogous reactions of **1** with a slight excess of the phosphines $P(C_6H_4Me\text{-}4)_3$ and $P(C_6H_2Me_2\text{-}3,5\text{-}OMe\text{-}4)_3$ proceeded similarly in dichloromethane at room temperature to afford the mono-substituted clusters $Mo_2Ir_2(\mu\text{-}CO)_3(CO)_6(L)(\eta^5\text{-}C_5H_5)_2$ [L = $P(C_6H_4Me\text{-}4)_3$ (**3**), $P(C_6H_2Me_2\text{-}3,5\text{-}OMe\text{-}4)_3$ (**4**)] in good yield following thin-layer chromatography (Scheme 1). A similar reaction with $AsPh_3$ gave the first arsine-functionalized

tetrahedral molybdenum-iridium cluster, $Mo_2Ir_2(\mu\text{-}CO)_3(AsPh_3)(CO)_6(\eta^5\text{-}C_5H_5)_2$ (**5**), in moderate yield (Scheme 2). Clusters **3**-**5** were characterized by a combination of IR, ESI mass spectrometry, ^1H and (in the case of **3** and **4**) ^{31}P NMR spectroscopy; the structures of **4** and two co-crystallized isomers of **5** (**5a** and **5b**) were confirmed by single-crystal X-ray diffraction studies. The IR spectra of **2**-**5** each contain seven bands, with very similar intensity distribution and frequencies, consistent with the clusters possessing the same solution structures. The ^1H NMR spectra of **3**-**5** contain resonances corresponding to the phosphine/arsine substituents together with a singlet for the cyclopentadienyl groups, while the ESI mass spectra contain proton or sodium adducts of the molecular ion. The ^{31}P NMR spectra contain broad resonances indicative of ligand fluxionality; this was examined further via variable temperature NMR studies (see below).

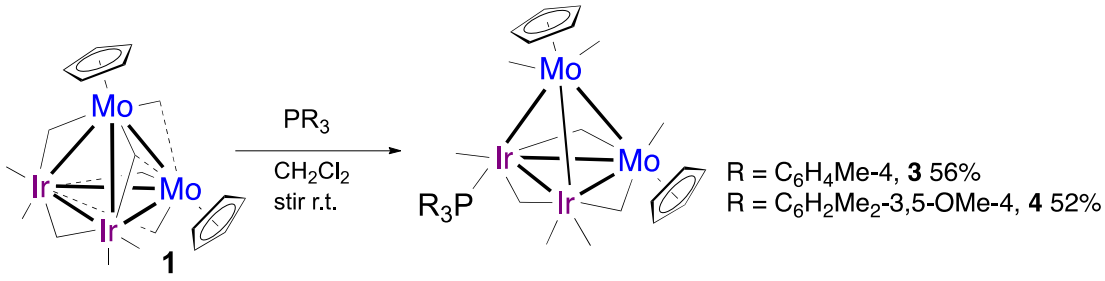

Scheme 1. Syntheses of $Mo_2Ir_2(\mu\text{-}CO)_3(CO)_6\{P(C_6H_4Me\text{-}4)_3\}(\eta^5\text{-}C_5H_5)_2$ (**3**) and $Mo_2Ir_2(\mu\text{-}CO)_3(CO)_6\{P(C_6H_2Me_2\text{-}3,5\text{-}OMe\text{-}4)_3\}(\eta^5\text{-}C_5H_5)_2$ (**4**).

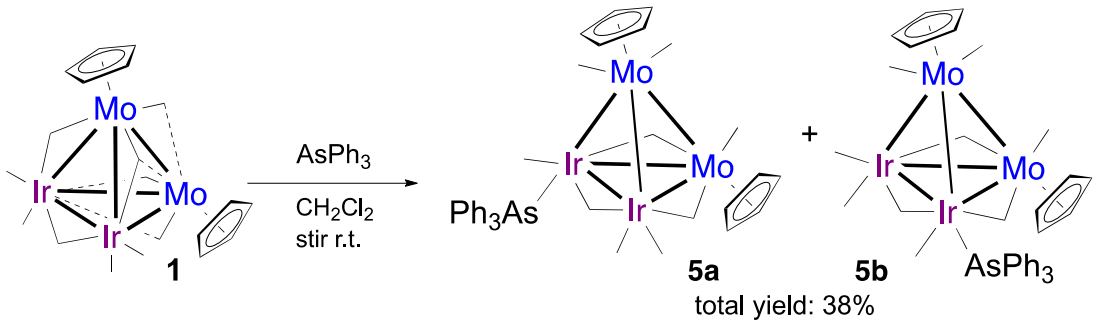

Scheme 2. Synthesis of $Mo_2Ir_2(\mu\text{-}CO)_3(AsPh_3)(CO)_6(\eta^5\text{-}C_5H_5)_2$ (**5a** and **5b**).

Single-crystal X-ray diffraction studies of **4** and two isomers of **5**, namely **5a** and **5b**, were undertaken. Crystal data are collected in Table S1 and selected bond distances are summarized in Table 1; ORTEP plots showing the molecular geometries and atomic labeling schemes are shown in Figures S1 (**4**), 1 (**5a**), and 2 (**5b**). All three structural studies reveal Mo_2Ir_2 pseudotetrahedral core geometries. In all three structures, the Mo atoms are ligated by η^5-cyclopentadienyl groups; the cluster coordination environments are completed by six terminal CO ligands, three bridging CO ligands arranged about a $MoIr_2$ plane, and an iridium-ligated phosphine/arsine, rendering both **4** and **5** electron precise by the effective atomic number rule [2 x 6(Mo) + 2 x 9(Ir) + 2 x 5(Cp) + 9 x 2(CO) + 2(ER_3) = 60 CVE]. The Mo_2Ir_2 core distances [Ir-Ir 2.7248(8) - 2.7267(5), Mo-Ir 2.812(2) – 2.9242(17), Mo-Mo 3.0761(8) – 3.097(3) Å] are within previously reported ranges for these linkages, while intracore bond angles are all close to 60°, as expected [**4**: 56.01(5) – 65.92(6)°; **5a**: 56.25(3) – 65.23(3)°; **5b**: 56.707(13) – 65.512(16)°]. Carbonyl ligands CO(12), CO(13), and CO(23) are in bridging sites about the Ir(1)Ir(2)Mo(3) plane in all three structures. CO(12) is symmetrically bridging in **4** and **5b**, but less so in **5a**, CO(13) is displaced towards Ir1 in **4** and **5a**, but towards Mo3 in **5b**, while CO(23) is displaced towards

Mo3 in **4** and **5a**, but towards Ir2 in **5b**; unsymmetrically bridging COs are a common feature in the structures of Mo/W-Ir carbonyl clusters [7,8,11].

The structural studies reveal that the phosphine/arsine ligands in **4**, **5a**, and **5b** are in axial coordination sites with respect to the plane of bridging carbonyls, similar to triphenylphosphine and trimethylphosphine in the structural studies of $Mo_2Ir_2(\mu\text{-}CO)_3(CO)_6(PPh_3)(\eta^5\text{-}C_5H_5)_2$ [24] and $Mo_2Ir_2(\mu\text{-}CO)_3(CO)_6(PMe_3)(\eta^5\text{-}C_5H_5)_2$ [9], respectively. In all three structures, the phosphine/arsine is *trans* to the Ir-Mo4 bond, but while the cyclopentadienyl is *trans* to this bond in **4** and **5b**, this is not the case in **5a**; thus, **5a** and **5b** are isomers resulting from differing disposition of the cyclopentadienyl group with respect to the arsine-Ir-Mo4 vector. We note that $Mo_2Ir_2(\mu\text{-}CO)_3(CO)_6(PMe_3)(\eta^5\text{-}C_5H_5)_2$ [9] is analogous to **5b** and $Mo_2Ir_2(\mu\text{-}CO)_3(CO)_6(PPh_3)(\eta^5\text{-}C_5H_5)_2$ [24] is analogous to **5a**, with respect to this cyclopentadienyl disposition. In related studies, comprehensive NMR and structural studies of the tungsten-containing homologues $W_2Ir_2(\mu\text{-}CO)_3(CO)_6(L)(\eta^5\text{-}C_5H_5)_2$ (L = PMe_3, PPh_3) [25] defined an isomer distribution comprised of analogous structures, the ligand disposition in the structural study of the PPh_3 adduct being the same as **5a**.

Table 1. Selected bond distances (Å) for **4**, **5a** and **5b**.

	4	**5a**	**5b**
Ir1-Ir2	2.7263(11)	2.7248(8)	2.7267(5)
Ir1-Mo3	2.9242(17)	2.8955(14)	2.8519(10)
Ir1-Mo4	2.8550(17)	2.8232(10)	2.8334(7)
Ir2-Mo3	2.812(2)	2.8401(9)	2.8845(7)
Ir2-Mo4	2.8789(19)	2.8957(10)	2.9065(8)
Mo3-Mo4	3.097(3)	3.0829(11)	3.0761(8)
Ir1-P1	2.367(4)		
Ir1-As1		2.4576(9)	
Ir2-As1			2.4403(7)
Ir1-C11	1.875(18)	1.853(7)	1.880(6)

Ir1-C12	2.132(17)	2.059(6)	2.101(5)
Ir2-C12	2.127(19)	2.140(6)	2.090(5)
Ir1-C13	2.030(16)	2.062(6)	2.181(6)
Mo3-C13	2.262(17)	2.249(6)	2.121(6)
Ir1-C14			1.893(6)
Ir2-C21	1.88(2)	1.872(7)	
Ir2-C22	1.88(2)	1.903(7)	1.873(6)
Ir2-C23	2.28(2)	2.245(6)	2.110(5)
Mo3-C23	2.05(2)	2.066(7)	2.161(6)
Mo3-C31	1.94(2)	1.981(8)	1.953(7)
Mo4-C41	1.97(2)	1.991(8)	1.990(6)
Mo4-C42	1.97(2)	1.987(7)	1.977(6)

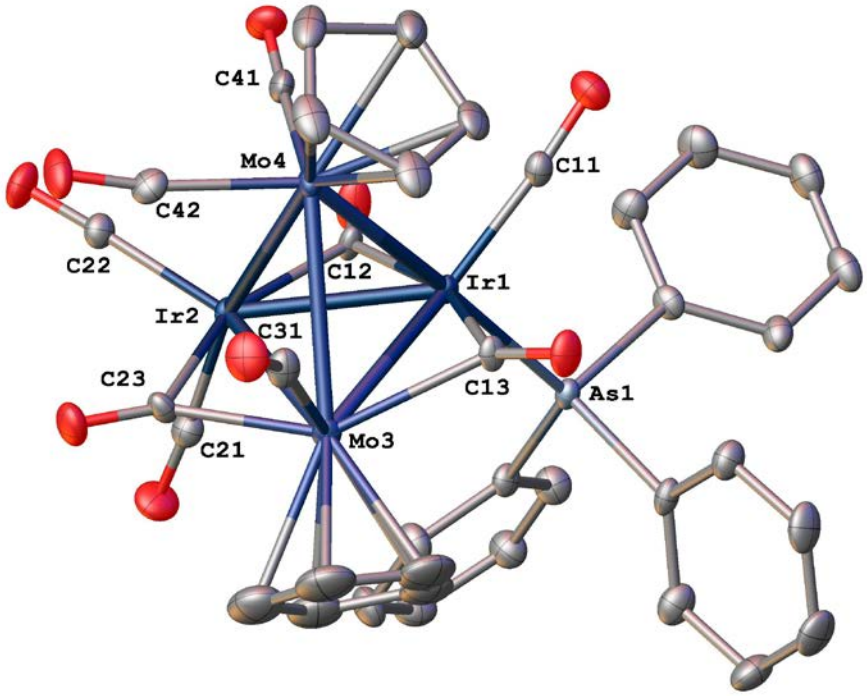

Figure 1. Molecular structure of $Mo_2Ir_2(\mu\text{-}CO)_3(AsPh_3)(CO)_6(\eta^5\text{-}C_5H_5)_2$ (**5a**), with thermal ellipsoids set at the 30% probability level. Hydrogen atoms have been omitted for clarity.

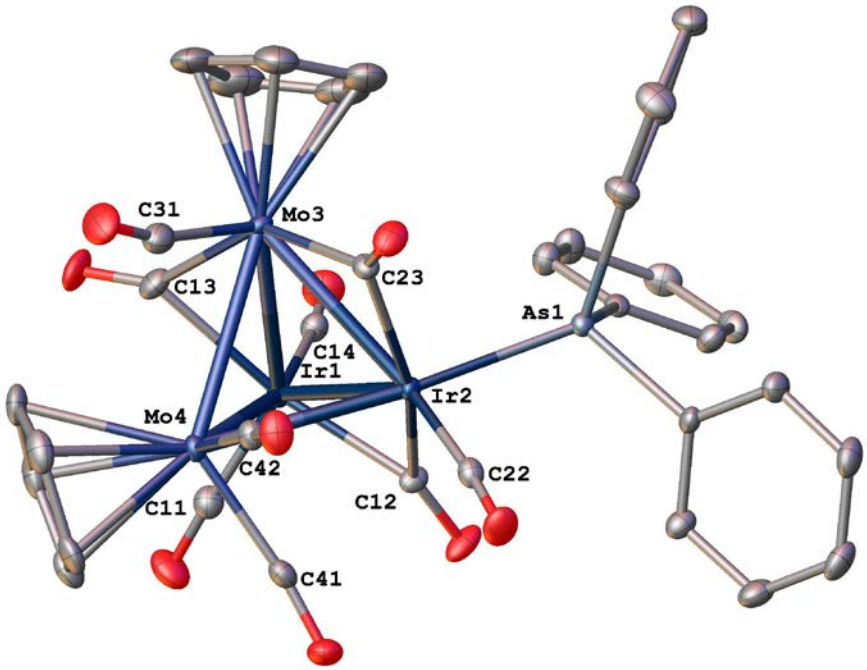

Figure 2. Molecular structure of $Mo_2Ir_2(\mu\text{-}CO)_3(AsPh_3)(CO)_6(\eta^5\text{-}C_5H_5)_2$ (**5b**), with thermal ellipsoids set at the 30% probability level. Hydrogen atoms have been omitted for clarity.

*3.2. Syntheses and structural studies of **6** and **8***

Reactions of **1** with internal and terminal alkynes generally proceed in refluxing dichloromethane to afford adducts corresponding to formal insertion into the Mo-Mo linkage in good yields [9-16]. An analogous reaction with ethynyltriisopropylsilane afforded the expected product $Mo_2Ir_2(\mu_4\text{-}\eta^2\text{-}HC_2SiPr^i_3)(\mu\text{-}CO)_4(CO)_4(\eta^5\text{-}C_5H_5)_2$ (**6**) in fair yield following thin-layer chromatography (Scheme 3). Cluster **6** was characterized by IR and ^{1}H NMR spectroscopy and ESI mass spectrometry, and its composition confirmed by a single-crystal X-ray diffraction study. The IR spectrum contains six ν(CO) bands, four in the terminal carbonyl region and two corresponding to edge-bridging carbonyl modes. The ^{1}H NMR spectrum contains a characteristic resonance corresponding to the ethynyl proton, together with signals resulting from the

cyclopentadienyl and isopropyl groups in the appropriate ratios, while the mass spectrum contains a protonated molecular ion signal.

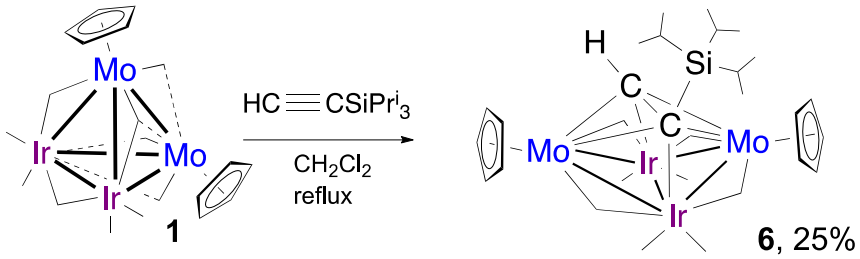

Scheme 3. Synthesis of $Mo_2Ir_2(\mu_4\text{-}\eta^2\text{-}HC_2SiPr^i_3)(\mu\text{-}CO)_4(CO)_4(\eta^5\text{-}C_5H_5)_2$ (**6**).

In contrast to **1**, reactions of $MoIr_3(\mu\text{-}CO)_3(CO)_8(\eta^5\text{-}C_5H_5)$ with internal or terminal alkynes have not thus far been reported. Reactions of the related $WIr_3(CO)_{11}(\eta^5\text{-}C_5H_5)$ with internal alkynes proceed in refluxing toluene to afford mixtures of clusters corresponding to alkyne dimerization and C≡C scission of the tetrahedral cluster [26], while reactions with terminal alkynes resulted only in decomposition [27]. We therefore explored the reaction of $MoIr_3(\mu\text{-}CO)_3(CO)_8(\eta^5\text{-}C_5H_5)$ with ethynyltrimethylsilane; this proceeded at room temperature to give a complex mixture of products in trace amounts. Reactions of phosphine-substituted molybdenum/tungsten-iridium carbonyl clusters with alkynes are thus far unexplored in both the molybdenum and tungsten systems, although the electronic and steric impact of the phosphine may be anticipated to influence reactivity. The reaction of $MoIr_3(\mu\text{-}CO)_3(CO)_6(PPh_3)_2(\eta^5\text{-}C_5H_5)$ (**7**) with ethynyltrimethylsilane was consequently studied, the reaction proceeding in refluxing dichloromethane to afford one product in fair yield following thin-layer chromatography (Scheme 4). Cluster **8** was characterized by the aforementioned techniques and a single-crystal X-ray diffraction

study. The IR spectrum contains a five-band ν(CO) pattern (three in the terminal and two in the bridging regions), the ESI mass spectrum contains a protonated molecular ion, and the ^{1}H NMR spectrum contains an ethynyl resonance at 7.65 ppm as well as the signals in the expected ratios for the phenyl, cyclopentadienyl, and methyl protons. The ethynyl resonance is downfield of the usual organic terminal acetylene region, but significantly upfield (ca. 2-3 ppm) of resonances for terminal alkyne adducts of **1** [9,12], presumably a result of the electron-releasing strength of the two phosphines (the ethynyl proton is indeed coupled to both phosphorus nuclei). The phosphorus nuclei each exhibit a singlet resonance in the ^{31}P{^{1}H} spectrum.

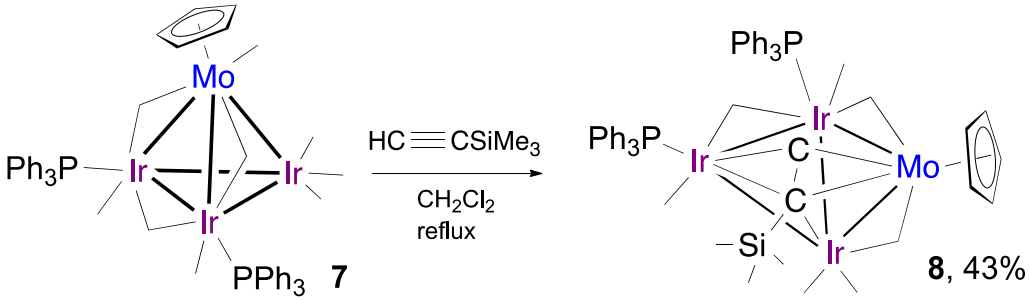

Scheme 4. Synthesis of $MoIr_3(\mu_4\text{-}\eta^2\text{-}HC_2SiMe_3)(\mu\text{-}CO)_3(CO)_4(PPh_3)_2(\eta^5\text{-}C_5H_5)$ (**8**).

Single-crystal X-ray diffraction studies of **6** and **8** were undertaken; crystal data are collected in Table S1 and selected bond distances are summarized in Table 2. ORTEP plots showing the molecular geometries and atomic labeling schemes are shown in Figures S2 (**6**) and 3 (**8**). Cluster **6** possesses a Mo_2Ir_2 butterfly core geometry in which the Mo-Mo linkage of the tetrahedral precursor has been cleaved. With each molybdenum ligated by cyclopentadienyl groups, four carbonyl ligands spanning the Mo-Ir linkages, each iridium bearing a further two carbonyl ligands, and the alkyne $\mu_4\text{-}\eta^2$-coordinated parallel to the Ir-Ir vector, it has the same core structure and ligand

disposition as many previously structurally-confirmed alkyne adducts of **1** [9,10,12-14,16]. The bond distances and angles are unexceptional compared to the extant analogous structurally-characterized clusters (in particular, the bridging carbonyls in the precedent structures display semi-bridging character with shorter Mo-C and longer Ir-C distances). Cluster **6** is two-electron deficient by the EAN rule (60 rather than 62 CVE), but electron precise by polyhedral skeletal electron-pair theory (seven pairs for a *closo* $Mo_2Ir_2C_2$ octahedron) [9].

Table 2. Selected bond distances (Å) for **6** and **8**.

	6 (M = Mo)	**8** (M = Ir)
Ir1-Ir2	2.6962(3)	2.7850(2)
Ir1-M3	2.7898(5)	2.7780(2)
Ir1-Mo4	2.7848(5)	2.8415(4)
Ir2-M3	2.8525(5)	2.7348(2)
Ir2-Mo4	2.8546(5)	2.7805(4)
Ir1-P1		2.3313(11)
Ir3-P2		2.3399(11)
Ir1-C134	2.129(5)	2.156(4)
M3-C134	2.293(5)	2.254(4)
Mo4-C134	2.297(5)	2.272(4)
Ir2-C234	2.119(5)	2.124(4)
M3-C234	2.428(5)	2.324(4)
Mo4-C234	2.385(5)	2.291(4)
C134-C234	1.454(7)	1.460(6)
Ir1-C11	1.918(7)	1.870(5)
Ir1-C12	1.926(6)	
Ir1-C13	2.267(6)	2.075(4)
M3-C13	2.005(7)	2.013(5)
Ir1-C14	2.261(5)	2.604(5)
Mo4-C14	2.003(6)	1.980(5)
Ir2-C21	1.913(7)	1.899(5)
Ir2-C22	1.930(6)	1.877(5)
Ir2-C23	2.474(6)	
Mo3-C23	1.973(6)	
Ir3-C31		1.839(5)
Ir2-C24	2.328(6)	2.236(5)
Mo4-C24	1.996(6)	2.027(5)

Cluster **8** also possesses a butterfly cluster core. The molybdenum is ligated by a cyclopentadienyl ligand, seven carbonyl ligands are arranged in terminal (four) and edge-bridging (three) sites, the wing-tip and one of the hinge iridium atoms bear triphenylphosphine ligands, and the alkyne is μ_4-η^2-bound parallel to the hinge Ir-Ir vector. The cluster bond lengths and angles are not unprecedented. The carbonyl ligands bridging the Mo-Ir linkages are semi-bridging with shorter Mo-C vectors, as in **6** above, while CO(13) is not formally semi-bridging, but again possesses a shorter bond to the wing-tip rather than hinge metal atom. Similar to **6**, cluster **8** is two-electron deficient by the EAN rule (60 rather than 62 CVE), but electron precise by polyhedral skeletal electron-pair theory (seven pairs for a *closo* $MoIr_3C_2$ octahedron).

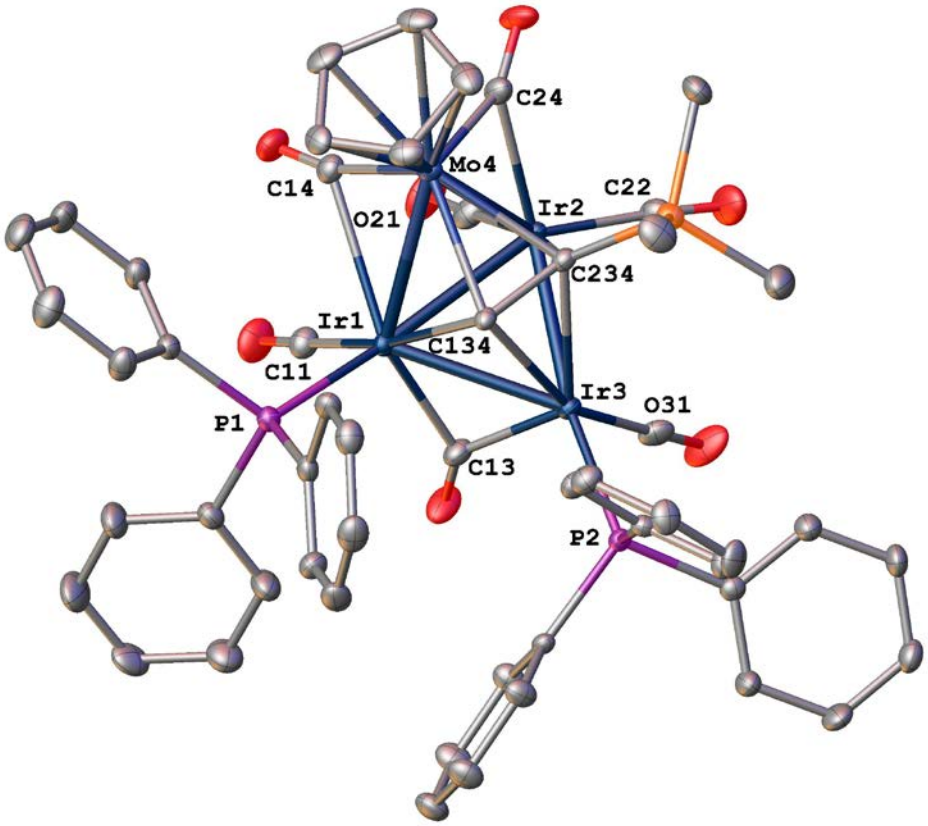

Figure 3. Molecular structure of $MoIr_3(\mu_4\text{-}\eta^2\text{-}HC_2SiMe_3)(\mu\text{-}CO)_3(CO)_4(PPh_3)_2(\eta^5\text{-}C_5H_5)$ (**8**), with thermal ellipsoids set at the 30% probability level. Hydrogen atoms have been omitted for clarity.

3.3. Electrochemical and spectroelectrochemical studies

Cyclic voltammetric scans of the tetrahedral complexes **2-5** show two successive one-electron oxidation processes [Table 3; a representative trace (that of **2**) is displayed in Figure 4]. In all cases, the first process is reversible (**2**, **5**) or semi-reversible (**3**, **4**), the same behavior being seen for **1** [11]. Thus, introduction of phosphine or arsine in proceeding from **1** to **2-5** results in an increase in ease of oxidation and increase in difficulty of reduction, as expected from the electron-releasing capacity of the phosphines/arsine compared to the carbonyl ligand. The alkyne-adduct **6** exhibits three oxidation processes; the first is reversible, unlike the subsequent two oxidations and the single reduction process observed within the scan window. Comparison to the CV data for the previously-reported phenylacetylene adduct $Mo_2Ir_2(\mu_4\text{-}\eta^2\text{-}HC_2Ph)(\mu\text{-}CO)_4(CO)_4(\eta^5\text{-}C_5H_5)_2$ [12] reveals that the electron-releasing aryl group affords an increase in ease of oxidation and increase in difficulty of reduction. Thus, both phosphine substitution and aryl substituent modification can be employed to systematically vary the electron richness of these clusters. Finally, progression from the aforementioned clusters to the iridium-rich bis(phosphine)-alkyne-adduct **8** results in an increasing difficulty in reduction and increased ease in oxidation, as anticipated, the latter affording access to five oxidation processes within the solvent window.

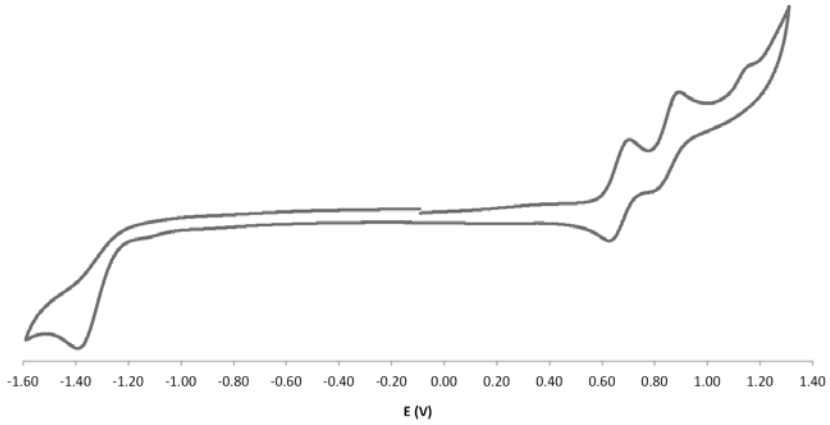

Figure 4. Cyclic voltammogram of ca. 10^{-3} M $Mo_2Ir_2(\mu\text{-}CO)_3(CO)_6(PPh_3)(\eta^5\text{-}C_5H_5)_2$ (**2**) in CH_2Cl_2 with 0.1 M $(NBu^n_4)PF_6$ as supporting electrolyte (scan rate 100 mV s^{-1}).

Table 3. Cyclic voltammetric data (V) for **1**-**6**, **8**.

	oxidations[a]	reductions[a]
	$E_{1/2}$ [ΔE (mV), i_{pc}/i_{pa}]	E_c
$Mo_2Ir_2(\mu\text{-}CO)_3(CO)_6(PPh_3)(\eta^5\text{-}C_5H_5)_2$ (**1**)[b]	0.84 [160, n.a.], 1.07	-1.24[c]
$Mo_2Ir_2(\mu\text{-}CO)_3(CO)_6(PPh_3)(\eta^5\text{-}C_5H_5)_2$ (**2**)	0.66 [60, 1], 0.85 [80, 0.5], 1.15	-1.38
$Mo_2Ir_2(\mu\text{-}CO)_3(CO)_6\{P(C_6H_4Me\text{-}4)_3\}(\eta^5\text{-}C_5H_5)_2$ (**3**)	0.66 [60, 0.8], 0.85 [60, 0.5], 1.12	-1.37
$Mo_2Ir_2(\mu\text{-}CO)_3(CO)_6\{P(C_6H_2Me_2\text{-}3,5\text{-}OMe\text{-}4)_3\}(\eta^5\text{-}C_5H_5)_2$ (**4**)	0.63 [80, 0.8], 0.86 [60, 0.4], 1.14	-1.34
$Mo_2Ir_2(\mu\text{-}CO)_3(AsPh_3)(CO)_6(\eta^5\text{-}C_5H_5)_2$ (**5**)	0.65 [50, 1], 0.93 [80, 0.4]	-1.33
$Mo_2Ir_2(\mu_4\text{-}\eta^2\text{-}HC_2SiPr^i_3)(\mu\text{-}CO)_4(CO)_4(\eta^5\text{-}C_5H_5)_2$ (**6**)	0.74 [60, 1], 1.06, 1.42	-1.20
$Mo_2Ir_2(\mu_4\text{-}\eta^2\text{-}HC_2Ph)(\mu\text{-}CO)_4(CO)_4(\eta^5\text{-}C_5H_5)_2$[d]	0.69 [60, 1], 0.96 [100, 0.85]	-1.33
$MoIr_3(\mu_4\text{-}\eta^2\text{-}HC_2SiMe_3)(\mu\text{-}CO)_3(CO)_4(PPh_3)_2(\eta^5\text{-}C_5H_5)$ (**8**)	0.49 [60, 1], 0.97 [90, 0.5], 1.22, 1.45, 1.66	-1.42

[a] All clusters exhibit irreversible processes except where indicated. [b] Reference [11]. [c] Two-electron process [11]. [d] Reference [12].

We have previously explored the UV-vis-NIR spectroelectrochemical behavior of $W_2Ir_2(CO)_{10}(\eta^5\text{-}C_5H_4Me)_2$ [11] (related to **1** by group 6 metal and cyclopentadienyl ligand variation) and $W_2Ir_2(\mu_4\text{-}\eta^2\text{-}PhC_2Me)(\mu\text{-}CO)_4(CO)_4(\eta^5\text{-}C_5H_4Me)_2$ [12] (related to **6** by group 6 metal, cyclopentadienyl ligand, and alkyne substituent variation) and found that the corresponding spectral progressions are relatively featureless, the spectra showing strong absorption at short wavelengths decreasing smoothly to weak absorption at long wavelengths, and with little variation across oxidation states. The reversible one-electron oxidation processes of selected examples in the present system have therefore been examined further by IR spectroelectrochemistry, likely to be a more sensitive tool of structural variation across the accessible oxidation states; representative traces are shown in Figures S3 (**2**), S4 (**6**), and 5 (**8**).

Oxidation of **2** results in progressive disappearance of the bridging carbonyl and lower energy terminal carbonyl bands [ν(CO) 1990 cm^{-1} - 1747 cm^{-1}], accompanied by the appearance of higher-energy terminal carbonyl bands. Oxidation of **6** and **8** similarly results in the appearance of bands at the high-energy end of the terminal carbonyl ν(CO) region, and reduction in intensity of bands in the bridging carbonyl region of the IR spectra. The ν(CO) bands therefore display a remarkable sensitivity to the cluster charge, and strongly suggest rearrangement following oxidation from species for which a “plane of bridging carbonyls” is significant to a predominantly “all-terminal” cluster CO distribution.

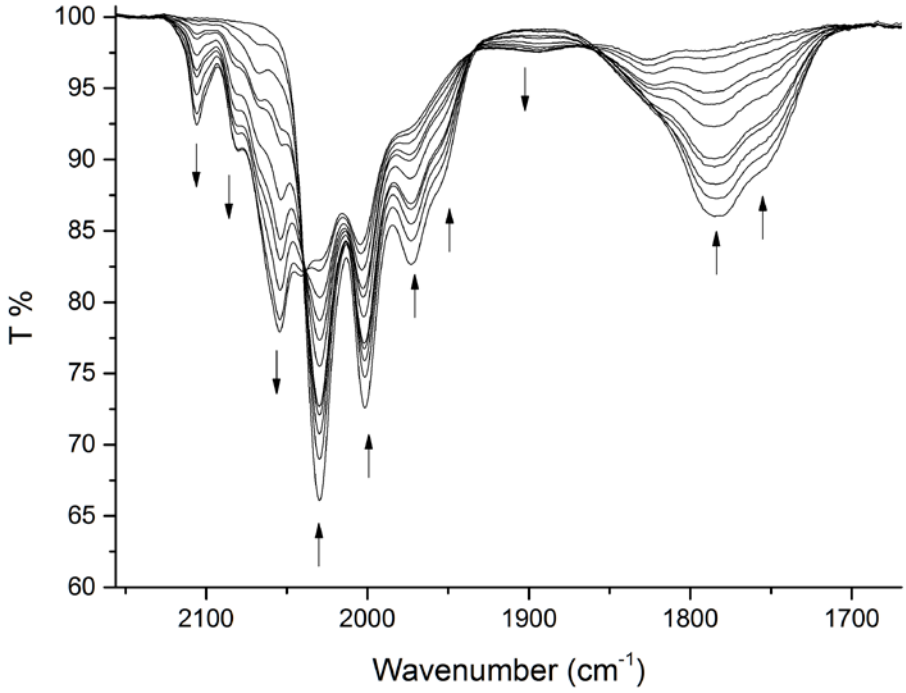

Figure 5. IR spectra of $MoIr_3(\mu_4\text{-}\eta^2\text{-}HC_2SiMe_3)(\mu\text{-}CO)_3(CO)_4(PPh_3)_2(\eta^5\text{-}C_5H_5)$ (**8**) (E_{appl} ca. +0.70 V) in CH_2Cl_2 with 0.3 M $(NBu^n_4)(PF_6)$ during exhaustive oxidation at 298 K.

3.4. Variable temperature ^{31}P NMR studies

We have previously reported that **2** is a mixture of interconverting isomers in solution at room temperature that is resolvable at low temperature [9]. The room temperature ^{31}P NMR spectra of **3** and **4** are also suggestive of the presence of interconverting isomers, so this possibility has been probed by variable temperature ^{31}P NMR studies, the resulting spectra being displayed in Figures S5 (**3**, $CDCl_3$), S6 (**4**, CD_2Cl_2), and 6 (**4**, toluene-d_8).

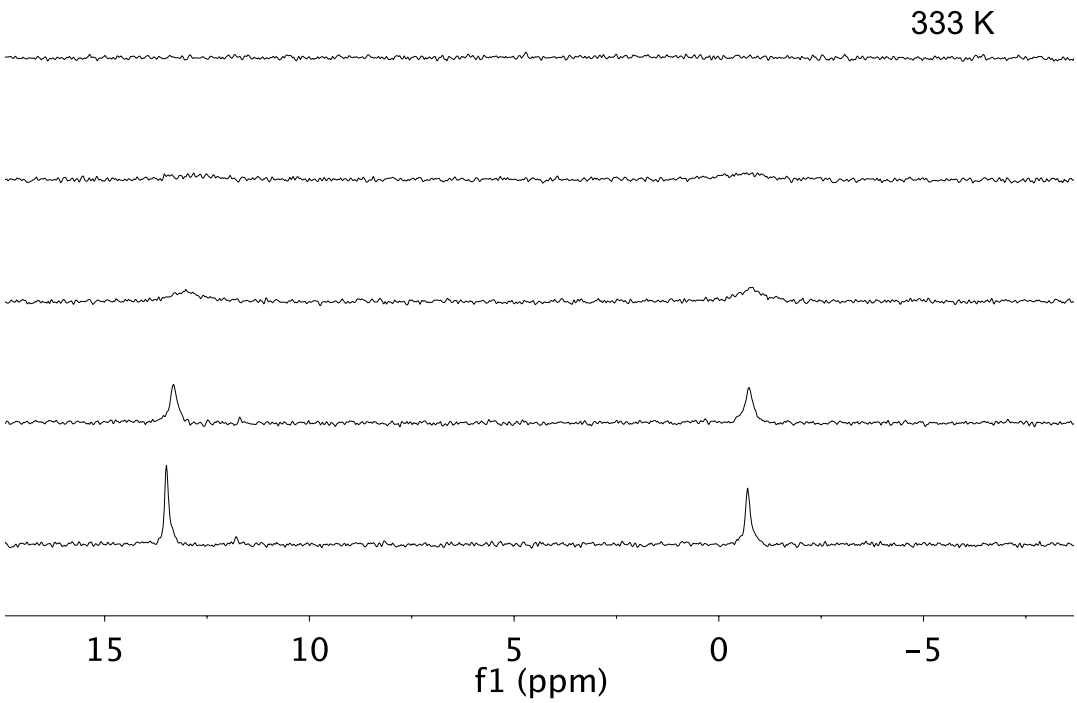

Figure 6. Variable-temperature ^{31}P NMR spectroscopic study of $Mo_2Ir_2(\mu\text{-}CO)_3(CO)_6\{P(C_6H_2Me_2\text{-}3,5\text{-}OMe\text{-}4)_3\}(\eta^5\text{-}C_5H_5)_2$ (**4**) in toluene-d_8 at 162 MHz.

Not surprisingly, the behavior of **3** and **4** are very similar to that of **2**, for which signals at 14.9 and 3.2 ppm in the ratio 1:2 were observed at 230 K in $CDCl_3$ [low-temperature limiting data: **3**, $CDCl_3$ (273 K): chemical shifts 12.6 and 1.0 ppm, ratio 1:2; **4**, toluene-d_8 (273 K): chemical shifts 13.5 and -0.7 ppm, ratio 1:1; **4**, CD_2Cl_2 (183 K): chemical shifts 12.7 and -1.3 ppm, ratio 3:2]. Thus, the resonances move upfield on increasing the electron-releasing strength of the phosphine [proceeding from PPh_3 (**2**) to $P(C_6H_4Me\text{-}4)_3$ (**3**) and $P(C_6H_2Me_2\text{-}3,5\text{-}OMe\text{-}4)_3$ (**4**)]. For **4**, the isomer ratio varies slightly on varying the solvent, and there is a small upfield shift of the resonances on increasing the solvent polarity (proceeding from toluene-d_8 to CD_2Cl_2). Comprehensive studies of the tungsten homologue of **2**, $W_2Ir_2(\mu\text{-}CO)_3(CO)_6(PPh_3)(\eta^5\text{-}C_5H_5)_2$, revealed that it consists of two interconverting isomers

[^{31}P NMR, CD_2Cl_2, 183K: chemical shifts 9.2 and -9.8 ppm, ratio 2:3] for which the downfield shift was assigned to a structure analogous to **5b** and the upfield shift was assigned to a structure analogous to **5a** [25]. We therefore tentatively assign the upfield and downfield ^{31}P NMR resonances of **2**-**4** in an analogous fashion. The coalescence seen on raising the temperature is consistent with a fluxional process interconverting the two isomers of each cluster. Studies with phosphine-substitution products in the tungsten-containing system have uncovered isomer interconversion via a "waggling" of a $W(CO)_2(\eta^5\text{-}C_5H_5)$ vertex or complete tripodal rotation at such a vertex [28]; such a process is also possible with **2**-**4** and would result in the observed fluxional behavior.

3.5. Optical limiting studies

The optical limiting properties of **2**-**5** and C_{60} were assayed using the Z-scan technique in dichloromethane at 532, 570 and 630 nm, the key data being summarized in Table 4. C_{60} was used as a reference to benchmark results for the new clusters, its data under our experimental conditions being provided for comparison. It is widely employed as a benchmark material so some brief comments about its performance are warranted. We note that much literature optical limiting data are as toluene solutions, but we have employed dichloromethane in the present studies because of the enhanced solubility of the clusters in this solvent. C_{60} has a greater ground-state absorption cross-section σ_0 in dichloromethane (4.8×10^{-18} cm^2) compared to toluene (3.7×10^{-18} cm^2 in toluene [29]). The effective excited-state cross-section σ_{eff} for C_{60} is lower in dichloromethane (11.4×10^{-18} cm^2 c.f. 27×10^{-18} cm^2 [28]), and so its figure-of-merit σ_{eff}/σ_0 in dichloromethane is lower than in toluene. The clamping

fluence of C_{60} in dichloromethane and toluene has been reported to be the same [30] although the data in dichloromethane were not presented (clamping fluence is the maximum fluence transmitted through the sample when increasing the input fluence); the clamping fluences at 532 nm (0.06 and 0.25 J cm^{-2} for solutions with 63% and 80% transmission, respectively) are consistent with the clamping fluence of our C_{60} solution with 70% transmission (0.1 J cm^{-2}).

Table 4. Optical limiting properties of **2**-**5** and C_{60}.

Measurement wavelength (nm)		Concentration (10^4 mol L^{-1})	Clamping fluence (J cm^{-1})	Extinction coefficient at measurement wavelength (M^{-1} cm^{-1})	Cross-section (10^{-18} cm^2)		Figure of merit σ_{eff}/σ_0	β_{eff} (10^{-6} cm W^{-1}) (± 20%)
					Ground state σ_0	Excited state σ_{eff}		
532	**2**	5.06	0.10	1820	6.95	9.78	1.41	3.8
532	**3**	5.44	0.13	1810	6.92	10.91	1.58	5.1
532	**4**	8.02	0.12	1390	5.31	8.60	1.62	5.7
532	**5**	10.95	0.12	1566	5.99	7.91	1.32	9.4
532	C_{60}	9.13	0.10	1270	4.85	11.40	2.35	8.2
570	**2**	7.12	0.09	1110	4.24	6.56	1.55	3.7
570	**3**	9.72	0.12	1020	3.89	6.66	1.71	5.1
570	**4**	14.10	0.12	850	3.24	5.65	1.74	7.2
570	**5**	10.10	0.12	1110	4.24	5.49	1.29	4.9
570	C_{60}	10.61	0.09	990	3.78	11.33	2.99	5.9
630	**2**	23.69	0.15	300	1.15	3.99	3.46	3.7

630	**3**	32.70	0.09	185	0.71	4.77	6.71	5.6
630	**4**	25.05	0.11	195	0.74	5.04	6.79	2.2
630	**5**	31.60	0.11	420	1.59	2.42	1.51	4.5
630	C_{60}	12.23	0.07	532	2.03	9.32	4.58	5.5

The UV-vis spectra for clusters **2-5** are shown in Figure 7. The spectra are broadly similar, with strong absorption at short wavelengths tending to weaker absorption at longer wavelengths, and a λ_{onset} at ca. 700 nm. The weak absorption through the region 500-650 nm suggests the possibility that these clusters could function as optical limiters by excited-state absorption.

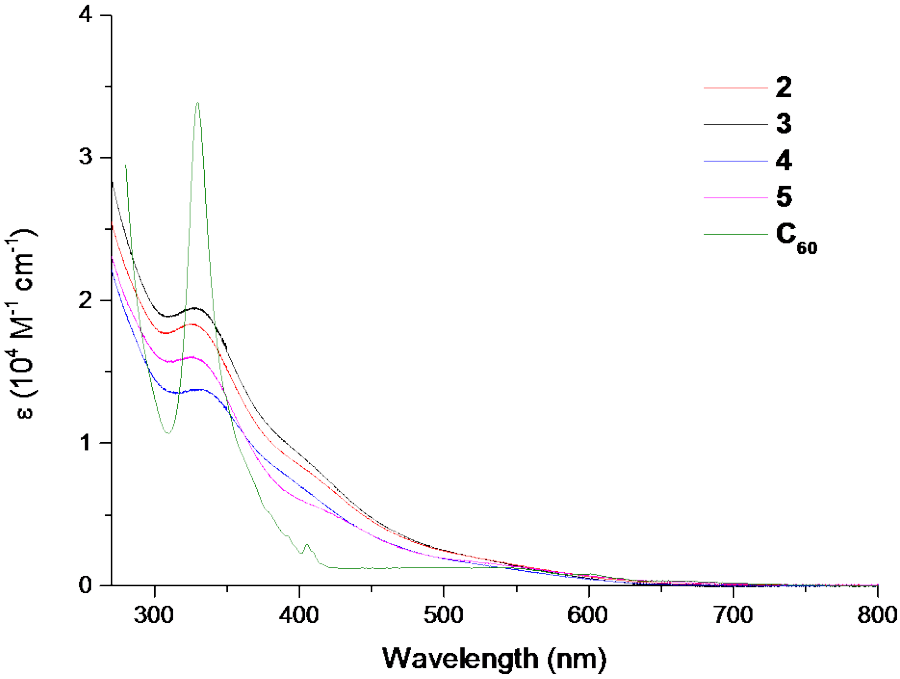

Figure 7. UV-Vis spectra of **2-5** and C_{60} in CH_2Cl_2.

Ground- and excited-state cross-sections at the measurement wavelengths and the UV-vis spectra are displayed in Figures S7 (**2**), S8 (**3**), S9 (**4**), S10 (**5**), and S11 (C_{60}). At the benchmark wavelength of 532 nm, **2-5** possess similar linear absorptivity, and therefore similar ground-state absorption cross-sections of ca. 4.8-6.9 x 10^{-18} cm^2. The σ_{eff}/σ_0 figures-of-merit at this wavelength follow the trend **4** > **3** > **2** > **5**, which parallels the electron-releasing strength of the phosphines/arsine. The excited-state cross-sections of **2-5** are in fact larger than the respective ground-state cross-sections

at all wavelengths surveyed, which suggests the compounds have potential as broadband optical limiters. Proceeding from 532 nm to 570 nm, all clusters except **5** increase their figure-of-merit, while at 630 nm, a wavelength at which they have low ground-state absorption cross-sections, **3** and **4** have σ_{eff}/σ_0 ratios larger than that of C_{60}.

The approximate clamping fluence has also been tabulated to afford a different perspective on the beam attenuation; the results are collected in Table 4 and the depicted in Figures 8 (**2**), S12 (**3**), S13 (**4**), S14 (**5**), and S15 (C_{60}). Under optical limiting conditions, the transmitted fluence is effectively clamped to a certain threshold value. Effective optical limiters tend to have low clamping fluence, as can be seen by the values shown for C_{60}. Cluster **2** has the lowest clamping fluence at 532 and 570 nm, matching that of C_{60}, while **3-5** have similar values at these wavelengths and are slightly poorer optical limiters than **2** or C_{60} (while being mindful of error margins). In contrast, **2** is the poorest performer of **2-5** at 630 nm, with **3** having the lowest threshold, similar to that of C_{60}.

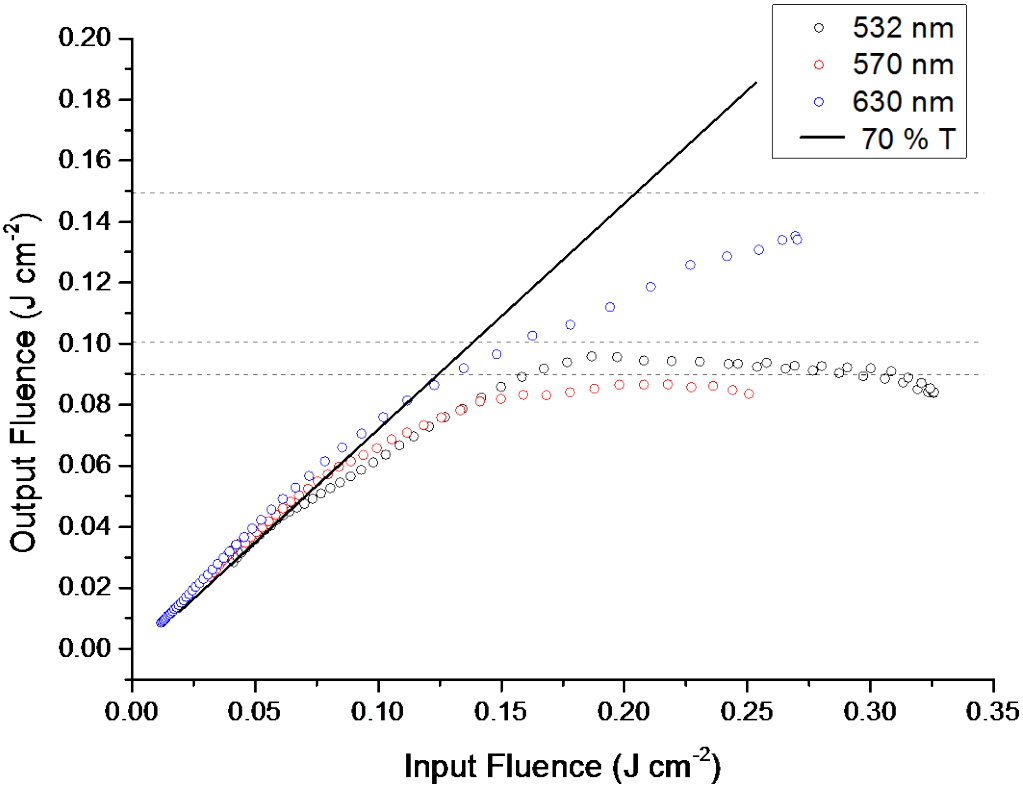

Figure 8. Optical limiting of **2** at the three wavelengths sampled [532 nm (black), 570 nm (red) and 630 nm (blue)]. The solid line is the 70 % transmission trend and the dotted lines are the approximate clamping fluences.

The values for the "effective" nonlinear absorption coefficient β_{eff} quantify nonlinear absorption from several possible processes (because pulse widths of the order of nanoseconds, such as employed in the present studies, integrate contributions from a variety of mechanisms including nonlinear absorption). At the benchmark wavelength of 532 nm, **2** has the smallest β_{eff} value (3.8 x 10^{-6} cm W^{-1}), **3** and **4** are similar in magnitude (5.6 x 10^{-6} cm W^{-1}), and **5** has the highest value, surpassing C_{60} (9.4 and 8.2 x 10^{-6} cm W^{-1}, respectively). The β_{eff} values for **2**, **5**, and C_{60} reduce on proceeding to longer measurement wavelengths, while **4** peaks at 570 nm and is reduced considerably at 630 nm, and the β_{eff} value for **3** is maximized at 630 nm. The

errors associated with such measurements (typically ± 20%) and the likely combination of mechanisms affording the observed optical limiting effects renders further speculation of comment unwarranted.

4. Conclusion

In the studies summarized above, ligand substitution at the tetrahedral cluster $Mo_2Ir_2(\mu_3\text{-}CO)(\mu\text{-}CO)_5(CO)_4(\eta^5\text{-}C_5H_5)_2$ has been expanded to embrace triphenylarsine and more-electron releasing phosphines, with several new clusters being X-ray structurally authenticated. The resultant clusters exist as mixtures of two isomers that are suggested to correspond to differing orientations of the $Mo(CO)_2(\eta^5\text{-}C_5H_5)$ vertex based on structural data of the arsine-containing isomers. The NMR data are consistent with the isomers interconverting by a "waggling" of this vertex or a complete tripodal rotation. Relatively clean alkyne insertion into the Mo-Mo bond of $Mo_2Ir_2(\mu_3\text{-}CO)(\mu\text{-}CO)_5(CO)_4(\eta^5\text{-}C_5H_5)_2$ has been documented extensively in the past, and a further example has been provided in the present work. The molybdenum-triiridium analogue alkyne chemistry was previously unexplored, but presumed to be less specific based on experience with tungsten-iridium clusters which usually afford mixtures; a molybdenum-containing example has now been examined herein and the presumed lack of reaction specificity has been confirmed. The present studies have shown that, in contrast, the bis(phosphine) derivative reacts by relatively clean insertion into a Mo-Ir bond to form a pseudo-octahedral adduct.

Electrochemical studies of these clusters have shown that cluster core electron richness is tunable in a rational fashion by ligand substitution and alkyne substituent modification, while IR spectroelectrochemical studies have revealed a decreasing proclivity for bridging carbonyls following oxidation. Finally, Z-scan studies have shown that the phosphine- and arsine-substituted clusters function as optical power limiters at several wavelengths in the visible region, with efficiencies similar to that of the benchmark material C_{60}.

Acknowledgements

We thank the Australian Research Council (ARC) for support of this work. J.F. is the recipient of a China Scholarship Council ANU Postgraduate Scholarship and M.P.C. holds an ARC Australian Research Fellowship.

References

[1] P. Braunstein, L. A. Oro, P. R. Raithby, Metal Clusters in Chemistry, Wiley-VCH, Weinheim, Germany, 1999.

[2] R. D. Adams, F. A. Cotton, Catalysis by Di- and Polynuclear Cluster Complexes, Wiley-VCH, New York, 1998.

[3] F. G. A. Stone, Angew. Chem., Int. Ed. Engl. 23 (1984) 89.

[4] H. Vahrenkamp, Comments Inorg. Chem. 4 (1985) 253.

[5] H. Vahrenkamp, Adv. Organomet. Chem. 22 (1983) 169.

[6] S. M. Waterman, N. T. Lucas, M. G. Humphrey, Adv. Organomet. Chem. 46 (2000) 47.

[7] N. T. Lucas, M. G. Humphrey, D. C. R. Hockless, J. Organomet. Chem. 535 (1997) 175.

[8] N. T. Lucas, I. R. Whittall, M. G. Humphrey, D. C. R. Hockless, M. P. S. Perera, M. L. Williams, J. Organomet. Chem. 540 (1997) 147.

[9] N. T. Lucas, M. G. Humphrey, P. C. Healy, M. L. Williams, J. Organomet. Chem. 545-546 (1997) 519.

[10] N. T. Lucas, M. G. Humphrey, A. D. Rae, Macromolecules 34 (2001) 6188.

[11] N. T. Lucas, J. P. Blitz, S. Petrie, R. Stranger, M. G. Humphrey, G. A. Heath, V. Otieno-Aledo, J. Am. Chem. Soc. 124 (2002) 5139.

[12] N. T. Lucas, E. G. A. Notaras, M. P. Cifuentes, M. G. Humphrey, Organometallics 22 (2003) 284.

[13] N. T. Lucas, E. G. A. Notaras, S. Petrie, R. Stranger, M. G. Humphrey, Organometallics 22 (2003) 708.

[14] E. G. A. Notaras, N. T. Lucas, M. G. Humphrey, A. C. Willis, A. D. Rae, Organometallics 22 (2003) 3659.

[15] A. J. Usher, M. G. Humphrey, A. C. Willis, J. Organomet. Chem. 682 (2003) 41.

[16] M. D. Randles, N. T. Lucas, M. P. Cifuentes, M. G. Humphrey, M. K. Smith, A. C. Willis, M. Samoc, Macromolecules 40 (2007) 7807.

[17] M. R. Churchill, Y. Li, J. R. Shapley, D. S. Foose, W. S. Uchiyama, J. Organomet. Chem. 312 (1986) 121.

[18] R. H. Blessing, Acta Crystallogr. Sect. A: Fundam. Crystallogr. 51 (1995) 33.

[19] P. Coppens in *Crystallographic Computing* ed F.R. Ahmed, S.R. Hall and C.P. Huber, Copenhagen, Munksgaard, (1970) pp 255-270.

[20] G. M. Sheldrick, Acta Crystallogr., Sect. A: Fundam. Crystallogr. 64 (2008) 112.

[21] G. M. Sheldrick, Acta Crystallogr., Sect. C: Struct. Chem. 71 (2015) 3.

[22] O. V. Dolomanov, L. J. Bourhis, R. J. Gildea, J. A. K. Howard, H. Puschmann, J. Appl. Cryst. 42 (2009) 339.

[23] P. van der Sluis, A. L. Spek, Acta Crystallogr., Sect. A: Fundam. Crystallogr., 46 (1990) 194.

[24] M. D. Randles, V. Gupta, P. V. Simpson, G. J. Moxey, A. L. Criddle, R. Stranger, M. P. Cifuentes, M. G. Humphrey, Polyhedron 52 (2013) 957.

[25] S. M. Waterman, M. G. Humphrey, J. Lee, G. E. Ball, D. C. R. Hockless, Organometallics 18 (1999) 2440.

[26] J. R. Shapley, M. G. Humphrey, C. H. McAteer, in Selectivity in Catalysis; ACS Symposium Series; M. Davis, S. Suib, Eds; American Chemical Society: Washington, DC, 1993; Vol. 517, Chapter 9.

[27] S. M. Waterman, M. G. Humphrey, V.-A. Tolhurst, M. I. Bruce, P. J. Low, D. C. R. Hockless, Organometallics 17 (1998) 5789.

[28] S. M. Waterman, M. G. Humphrey, J. Lee, J. Organomet. Chem. 589 (1999) 226.

[29] J. Callaghan, W. J. Blau, F. Z. Henari, J. Nonlinear Opt. Phys. Mater. 4 (2000) 505.

[30] L. W. Tutt, A. Kost, Nature 365 (1992) 225.